JACS
JOURNAL OF THE AMERICAN CHEMICAL SOCIETY
pubs.acs.org/JACS
Communication

# Rosette Nanotube Porins as Ion Selective Transporters and Single-Molecule Sensors

Prabhat Tripathi, Liang Shuai, Himanshu Joshi, Hirohito Yamazaki, William H. Fowle, Aleksei Aksimentiev,* Hicham Fenniri,* and Meni Wanunu*

Cite This: J. Am. Chem. Soc. 2020, 142, 1680−1685
Read Online
ACCESS | Metrics & More | Article Recommendations | Supporting Information

**ABSTRACT:** Rosette nanotubes (RNTs) are a class of materials formed by molecular self-assembly of a fused guanine−cytosine base (G∧C base). An important feature of these self-assembled nanotubes is their precise atomic structure, intriguing for rational design and optimization as synthetic transmembrane porins. Here, we present experimental observations of ion transport across 1.1 nm inner diameter RNT porins (RNTPs) of various lengths in the range 5−200 nm. In a typical experiment, custom lipophilic RNTPs were first inserted into lipid vesicles; the vesicles then spontaneously fused with a planar lipid bilayer, which produced stepwise increases of ion current across the bilayer. Our measurements in 1 M KCl solution indicate ion transport rates of ∼50 ions $s^{-1}$ $V^{-1}$ m, which for short channels amounts to conductance values of ∼1 nS, commensurate with naturally occurring toxin channels such as α-hemolysin. Measurements of interaction times of α-cyclodextrin with RNTPs reveal two distinct unbinding time scales, which suggest that interactions of either face of α-cyclodextrin with the RNTP face are differentiable, backed with all-atom molecular dynamics simulations. Our results highlight the potential of RNTPs as self-assembled nonproteinaceous single-molecule sensors and selective nanofilters with tunable functionality through chemistry.



Intrigued by nature's biochemical machinery,[1,2] scientists have been trying to create *de novo* design of transmembrane channels that can be engineered and tuned to exhibit selective transport of ions and molecules, sense and recognize specific chemicals/biomolecules, and behave as actuatable gates that open and close in response to various stimuli.[3] Indeed, numerous conventional building blocks such as polypeptides[4,5] and organic polymers[6] have been used to produce mimics of biological channels and transporters, although *de novo* design is enormously challenging because polymer folding is often difficult to predict and poor solubility in water can complicate experiments.[7,8] While several examples of self-assembled supramolecular structures were produced,[9−11] single-molecule sensing using these pores was not demonstrated, presumably because of their small size (<100 pS conductance values were found in 1−2 M KCl electrolytes). To generate larger self-assembled pores, origami-based folding of DNA into well-defined and predictable transmembrane channels has been achieved recently[12−14] and further utilized for single-molecule sensing.[15] However, issues that remain with DNA-based nanopores include the high cost and low yield of manufacturing the DNA precursors, possibilities of misfolding via incorrect hybridization to the staple DNA oligomers, and ion leakage through the skeleton of the DNA pores.[16,17] Recent studies suggest that a DNA duplex spanning the lipid bilayer can also produce an ion current,[18] further proving the leaky nature of DNA-lipid interface to ions.[19] In principle, for *de novo* design of transmembrane channels, molecular building blocks should be as small as possible and should be organized together with strong forces to provide a stable, rigid, and well-defined nanostructure.

The discovery of hierarchical self-assembly of heteroaromatic bicyclic G∧C base (Figure 1A) allows us to create

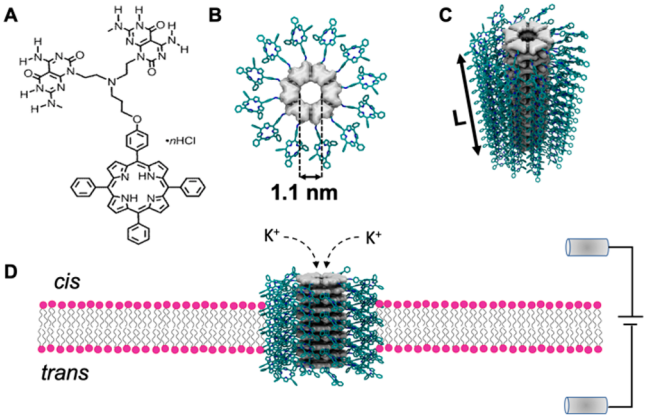


**Figure 1.** Synthetic rosette nanotube porins (RNTPs) in lipid bilayer de novo from fused G∧C base. (A) Chemical structure of fused porphyrin modified G∧C base. (B) Top view of rosette stack formed via hydrogen bonding of six G∧C bases. (C) Perspective view of an RNTP of length *L*, formed by π−π stacking of several rosettes. (D) RNTP insertion into the lipid bilayer results in a water-filled RNTP lumen. Application of voltage across the membrane results in ion flow across the pore, as shown here for $K^+$ ions.

**Received:** October 14, 2019
**Published:** January 8, 2020




https://dx.doi.org/10.1021/jacs.9b10993
J. Am. Chem. Soc. 2020, 142, 1680−1685

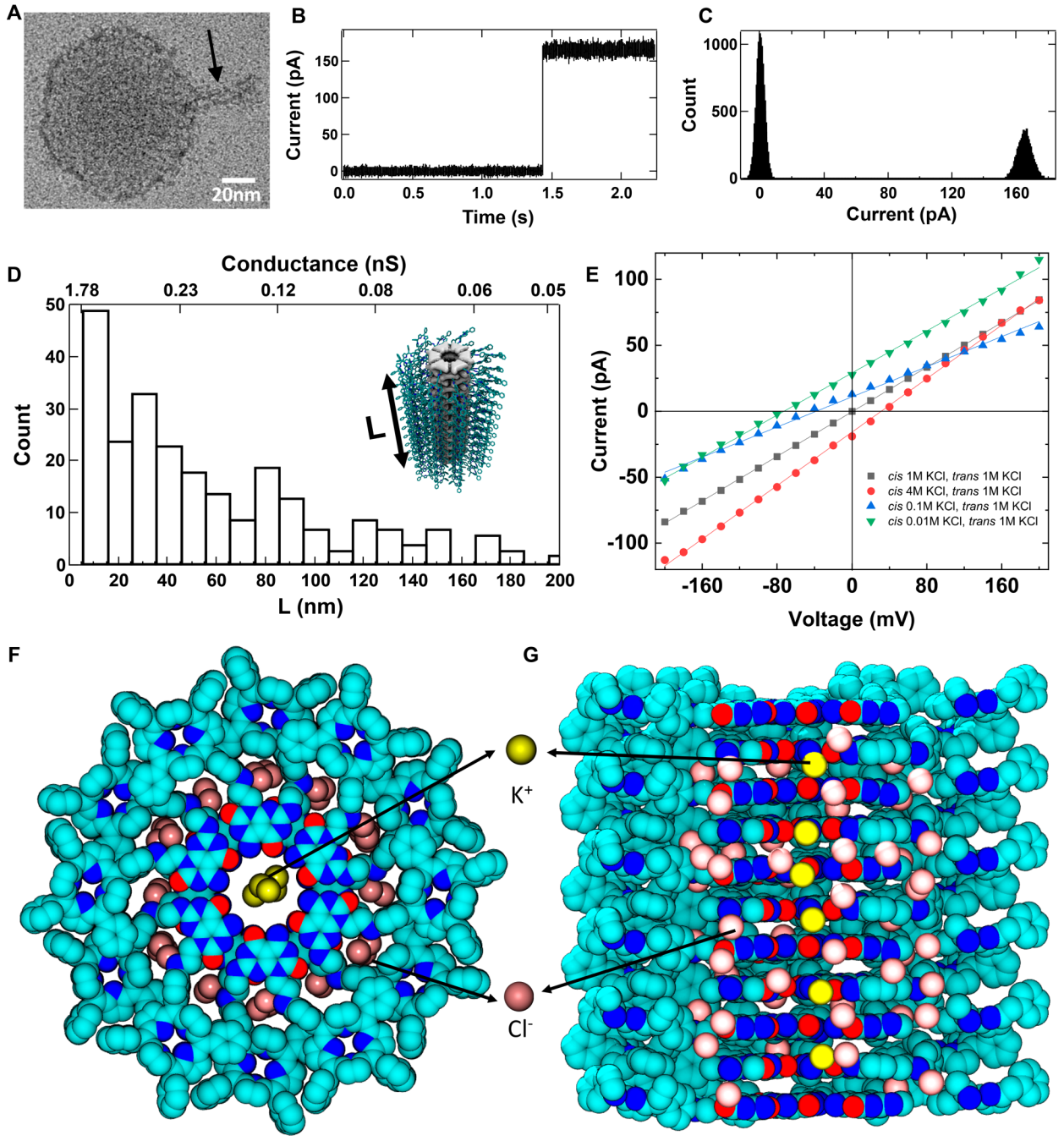


**Figure 2.** Ion conductance of RNTPs. (A) Representative TEM image of an ~40 nm long RNTP reconstituted in a lipid vesicle (see black arrow). (B) Observation of a stepwise increase in ion current due to incorporation of single RNTP in lipid-bilayer of estimated length 5.5 nm. The traces shown here were recorded at 1 M KCl, 10 mM HEPES, pH 7.5 at 100 mV, and current signal was low-pass filtered at 5 kHz (C) All-point histogram of the current trace shown in (B). (D) Histogram of estimated RNTP lengths ($L$) based on data from 257 insertions. (E) Current vs voltage for different salt conditions for an ~25 nm long RNTP. A snapshot from the all-atom MD simulation of a 5 nm long RNTP showing the (F) top and (G) side views. The non-hydrogen atoms of RNTP are shown as spheres colored according to atom type (carbon in cyan, nitrogen in blue, oxygen in red); $Cl^-$ and $K^+$ are shown as pink and yellow spheres, respectively. Water and lipid molecules are not shown for clarity. The snapshot shows that the cations are only present in the central channel lumen, and the anions are distributed in the periphery of the channel. The simulation explains the weak selectivity of RNTP toward $K^+$ transport due to binding of $Cl^-$ to positively charged ammonium groups at the junction of G∧C bases and porphyrin.

predictable and rigid rosette nanotube porins (RNTPs) with tunable dimensions and chemical/physical properties.[20,21] RNTPs can be promising alternatives to top-down pore structures, as the molecules that self-assemble into RNTPs are relatively straightforward. Recently, carbon nanotube porins have been incorporated in the lipid bilayer and in live cell membranes to explore water and ion transport.[22,23] Here, we measure the ion transport properties of RNTPs by creating synthetic channels constructed entirely from the self-assembly of bicyclic base G∧C, anchored into planar lipid bilayers through porphyrin side chains. The bicyclic system G∧C undergoes a hierarchical self-assembly process. First, it forms a


https://dx.doi.org/10.1021/jacs.9b10993
J. Am. Chem. Soc. 2020, 142, 1680−1685

six-membered rosette-like ring (Figure 1B), stabilized by 18 H-bonds.[20,21] Several rosette rings then organize via $\pi-\pi$ stacking to produce an arbitrary-length RNTP with an internal diameter of 1.1 nm, resulting in barrel-like architecture (Figure 1C).[21] Because of the presence of porphyrin moieties, the RNTPs easily partition into lipid bilayers and are insoluble in water. We overcome this challenge by following recently reported strategies,[12,22] and reconstituting porphyrin modified RNTPs into lipid vesicles, such that fusion of a vesicle into the lipid bilayer results in a transmembrane channel (Figure 1D). We find that RNTPs transport ions at rates of ~50 ions $s^{-1}$ $V^{-1}$ m, comparable to previously reported naturally occurring[1,3] and artificial channels,[4,12,15,22,23] despite the differences in electrostatic and hydrophobic environments of their inner space.

The synthesis of porphyrin-modified heteroaromatic bicyclic base G∧C is detailed in the Supporting Information (SI) (section S1A). Transmission electron microscopy (TEM) images of RNTP samples established their tubular structure and dimensions (SI: section S1E, Figure S2A, S2B). We purified RNTP samples (SI: section S1B and Figure S2B) to obtain RNTPs shorter in length and reconstituted them in lipid vesicles (section S1C). TEM imaging of RNTPs reconstituted in lipid vesicles show that the RNTPs can stick to lipid bilayer membranes as shown in Figure 2A and Figure S3.

To insert RNTPs in the lipid bilayer and explore the transport properties, we formed a planar lipid bilayer using the Montal−Mueller technique (section S1D) on a 50−100 $\mu$m aperture on PTFE film separating two-compartment cis/trans, each containing 1 M KCl, 10 mM HEPES, and pH 7.5, and applied an electric potential to the *trans* compartment, keeping *cis* grounded (Figure 1D). Upon addition of 2−5 $\mu$L of a solution of RNTP reconstituted in the vesicle, we observed a stepwise increase in ionic current. We did not observe any ionic current upon addition of vesicles alone. This suggest that the observed stepwise increase in ionic current with RNTP-reconstituted vesicles must be due to the insertion of RNTP in the lipid bilayer. Typical ionic current traces, manifesting the spontaneous insertion of single RNTP in the lipid bilayer, are shown in Figure 2B and in Figure S4A. Notably, the stepwise jumps in ionic current are not identical in magnitude (Figure S4B), which we attribute to insertions of RNTPs with different lengths. We quantified the length of the inserted RNTPs by measuring the conductance of each inserted channel. The differences in peak positions in the histograms of current traces were taken as single channel currents (Figures 2C, S4A(ii)). The length of inserted RNTPs can be estimated from the conductance of the channels using well-known analytical equations.[24] For example, in Figure 2B, the ionic current jumps from 0.4 ± 0.01 pA to 165 ± 0.04 pA, when an RNTP of conductance 1.64 nS is inserted ($L \approx 5.5$ nm). The inserted RNTP length distribution ($n = 257$) is shown in Figure 2C. We performed finite-element COMSOL simulations (Figure S5) to further reinforce the conductance/length relationship in these RNTPs.

Our results have shown that most of the inserted RNTPs are short, less than 20 nm, and have a conductance of 1−2 nS (Figure 2D), similar values to biological toxin channels and other reported artificial channels.[4,12,15,22,23] In more than 90% of RNTP insertions, we observed stable and steady-state ionic currents with noise spectra similar to the case of $\alpha$-hemolysin channels[25] (Figure S6), and lower 1/f noise slopes than those for solid-state nanopores,[26,27] suggesting that RNTPs are suitable for single-molecule sensing. In less than 10% of cases, we observed unstable and highly stochastic ionic currents (Figure S7), where the conductance state of the RNTP fluctuates at different levels. We attribute this behavior to be due to RNTP mis-assembly and/or mechanical instability of an RNTP, akin to gating in biological channels and other synthetic porins such as carbon nanotube porins (CNTPs).[22,23] While in biological channels gating occurs mostly due to conformational changes of proteins, in the case of the RNTPs, gating can in principle be due to various reasons such as tilting in and out of the lipid bilayer (Figure S7(ii)). We also observed a class of events where ionic current due to the insertion of several RNTPs decreased in a stepwise manner (Figure S8(i)), as observed for DNA barrels in the lipid bilayer and interpreted as distinct pore closure events.[14] This effect can also be due to tilting of an RNTP such that the hydrophobic exterior of the RNTPs can be maximally exposed to the lipid environment, as predicted from simulation (see SI: section S8).[28]

We also explored the ion selectivity of RNTPs by measuring ionic currents at different transmembrane voltages and salt gradients (Figure 2E). As expected, the current−voltage relationship for RNTPs showed ohmic behavior at all salt conditions. Selectivity ratios ($P_{K^+}/P_{Cl^-}$) were calculated at different salt asymmetric conditions from the reversal potentials using the Goldman−Hodgkin−Katz equation (SI: section S9). As shown in Table 1, we found an ~2-fold preference for cations over anions at low salt concentrations (<100 mM) and virtually no selectivity at high salt concentration.

**Table 1. Reversal Potentials and Selectivity Ratios of RNTPs Measured under Different KCl Concentration Gradients (pH 7.5)**

| salt concn (cis/trans) | corrected $V_R$ (mV) | permselectivity | selectivity ratio ($K^+/Cl^-$) |
|---|---|---|---|
| 0.01 M/1 M | 37.9 | 0.35 | 2.03 |
| 0.1 M/1 M | 15.5 | 0.31 | 1.82 |
| 4 M/1 M | −2.7 | 0.09 | 1.17 |

To understand the weak cation selectivity, we used molecular dynamics[17] to simulate an all-atom model of an RNTP in a lipid bilayer and surrounded by electrolyte solution. The 150 ns MD trajectory of the system revealed preferential localization of $K^+$ ions at the center of the nanotube and the $Cl^-$ ion in the space between the G∧C bases and porphyrin moieties; see Figure 2F, G. Further analysis of the simulation results (SI: section S10) reveals on average 750 water molecules and 6 cations (either $Na^+$ or $K^+$) within the 5 nm long RNTP at steady state.

Finally, we investigated the potential of the RNTPs as robust single-molecule sensors. Here, we employed $\alpha$-cyclodextrins[29] ($\alpha$-CD, 200 $\mu$M) across the lipid bilayer containing RNTP and observed transient blockades in ionic current. We find that the frequency of ionic current blockades increases with increasing $\alpha$-CD concentrations (Figure 3A, B). A double exponential fit of the interevent times distribution (Figure S11(i)) indicates two distinct time constants. This suggests that the individual current blockade events are due to either arrival of single $\alpha$-CD molecule from bulk to the RNTP or binding/rebinding of the same $\alpha$-CD to the RNTP. We also observed current blockades at negative voltages (Figure 3D), suggesting that $\alpha$-CD:RNTP


https://dx.doi.org/10.1021/jacs.9b10993
J. Am. Chem. Soc. 2020, 142, 1680−1685

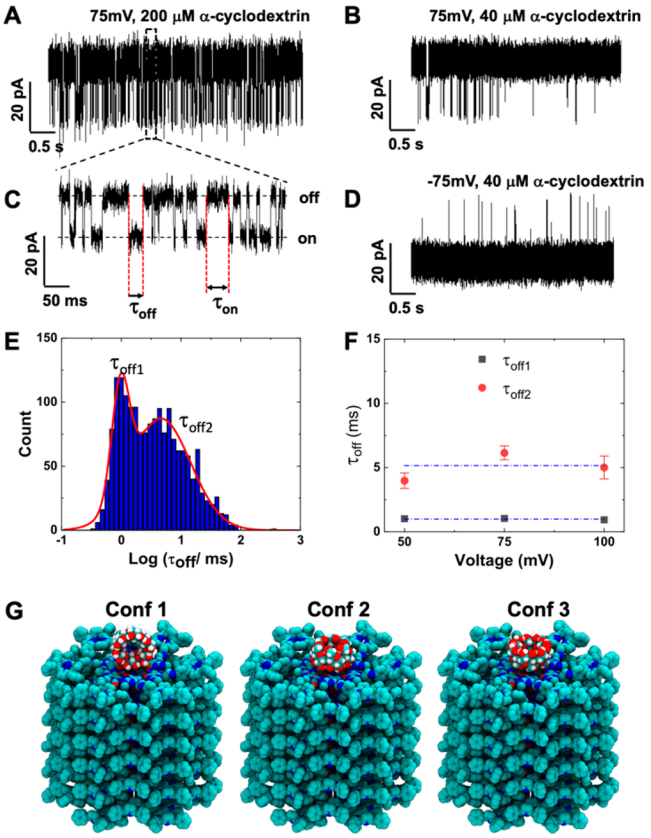


**Figure 3.** Single-molecule sensing of α-cyclodextrin (α-CD) with RNTP. (A) Trace of ionic current blockades induced by 200 μM α-CD at 75 mV. (B) Trace of ionic current blockades induced 40 μM α-CD at 75 mV. (C) Zoomed-in view of the trace in A, showing distinct current blockades induced by the interaction of α-CD with an RNTP. The lifetime $\tau_{off}$ is the duration of time α-CD stays at the RNTP ("on" state) before unbinding. The lifetime $\tau_{on}$ represents the time that α-CD takes to arrive and bind to the RNTP. (D) Trace showing ionic current blockades for 40 μM α-CD at −75 mV. Current traces shown in plots were recorded at 1 M KCl, 10 mM HEPES, pH 7.5, and low-pass filtered at 5 kHz. (E) Histogram of $\tau_{off}$ times, $n$ = 1752. Red curves represent the fit of histogram with a double-peak Gaussian function. (F) Peak positions of the histogram ($\tau_{off1}$ and $\tau_{off2}$) as a function of applied voltage. Error bars represent standard error obtained in fitting with two peak Gaussian function. (G) Snapshots from all-atom MD simulations of the three conformations (1, 2, and 3) of α-CD at the RNTP. The simulation results (see Figure 4) show that conformation 3 has strongest interaction with the RNTP. Blockade currents computed using the Steric Exclusion Model[34] (SI: section S15) for the various conformations are 18%, 51%, and 51% of the open pore value, consistent with our experimental data.

interactions are not voltage polarity dependent. The ionic current blockade lifetime, $\tau_{off}$ (Figure 3C), represents the α-CD residence time on the RNTP. The histogram of $\tau_{off}$ has a bimodal distribution with two time constants, ∼1 ms and ∼5 ms, respectively, and are independent of the applied voltage (Figure 3E, F). This is unlike a charged molecule, where residence times at the pore typically changes with voltage.[30] To understand the observed two types of residence time, we performed all-atom MD simulations of interaction between α-CD and RNTP. The molecular architecture of α-CD is a tapered cylindrical structure with outer diameters 1.46 and 1.37 nm, respectively (Figure 3G; SI: section S13). This suggests that α-CD cannot translocate through the RNTP, but can interact with three specific orientations as shown in Figure 3G.

We computed the free energy between an α-CD molecule and an RNTP for the approach of an α-CD molecule to an RNTP in three different orientations (Figure 4). Looking at the depth of the free energy well near the RNT entrance, we find that conformation 3 (see Figure 3G), in which the primary carbon of the glucose moieties interacts with the RNT face, has a higher affinity than the other two conformations. Consequently, we attribute the time constant $\tau_{off2}$ in Figure 3E to a binding mode representing conformation 3 and $\tau_{off1}$ to conformations 1 and/or 2.

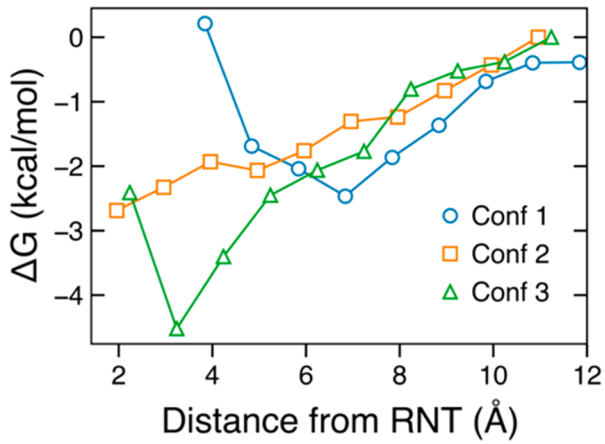


**Figure 4.** Energetics of α-CD and RNTP interactions. Free energy as a function of distance between the center-of-mass of α-CD and the top layer of an RNTP for three specific conformations shown in 3G (see text).

Our results establish RNTPs as promising *de novo* porins with predefined diameters. More work is needed to demonstrate controllable chemical and physical properties, as well as to improve porin lifetimes from several minutes to hours of operation. In addition, we have demonstrated here single-molecule sensing of α-CD, a chiral molecule, revealing differential interaction times for both faces of the molecule with the achiral RNTP face. We expect that RNTP improvements could lead to new porins with enhanced ion selectivity, which can pave the way to new directions for water purification applications, industrial-scale separations, or flexible reconfigurable nanofluidic circuits. For example, the inner channel of RNTP can be functionalized with a variety of hydrophobic, aromatic, or hydrophilic groups to further tune the selectivity (work in progress). Moreover, inserting one or two rings between the G and C faces of the G∧C base[31,32] should also allow for the design of transmembrane channel structures with larger pore diameters (1.4 and 1.7 nm) that can perhaps achieve single-file translocation and sequence-selective sensing of biopolymers such as nucleic acids and proteins.[33]

## ■ ASSOCIATED CONTENT

### Supporting Information

The Supporting Information is available free of charge at https://pubs.acs.org/doi/10.1021/jacs.9b10993.

Figure S1−S13, Table S1, supplementary methods, additional TEM images of RNTs and RNTPs reconstituted in vesicles, additional data and analysis of RNTP



https://dx.doi.org/10.1021/jacs.9b10993
J. Am. Chem. Soc. 2020, 142, 1680−1685

conductance, sensing data of α-CD, and MD simulation details (PDF)

## AUTHOR INFORMATION


### Corresponding Authors

**Aleksei Aksimentiev** − *University of Illinois at Urbana—Champaign, Urbana, Illinois;* orcid.org/0000-0002-6042-8442; Email: aksiment@illinois.edu

**Hicham Fenniri** − *Northeastern University, Boston, Massachusetts;* orcid.org/0000-0001-7629-7080; Email: h.fenniri@northeastern.edu

**Meni Wanunu** − *Northeastern University, Boston, Massachusetts;* orcid.org/0000-0002-9837-0004; Email: wanunu@neu.edu

### Other Authors

**Prabhat Tripathi** − *Northeastern University, Boston, Massachusetts*

**Liang Shuai** − *Northeastern University, Boston, Massachusetts*

**Himanshu Joshi** − *University of Illinois at Urbana—Champaign, Urbana, Illinois*

**Hirohito Yamazaki** − *Northeastern University, Boston, Massachusetts*

**William H. Fowle** − *Northeastern University, Boston, Massachusetts*

Complete contact information is available at: https://pubs.acs.org/10.1021/jacs.9b10993


### Notes

The authors declare no competing financial interest.

## ACKNOWLEDGMENTS

We would like to thank Xinqi Kang for her assistance with experiments with the lipid vesicles. We would like to thank Dr. Naresh Niranjan Dhanasekar for helpful discussions on TEM imaging of vesicles. This work was supported by the National Science Foundation (DMR-1710211, MW). H.J. and A.A. acknowledge support from the National Institutes of Health (P41-GM104601), National Science Foundation (DMR-1827346), and supercomputer time provided through XSEDE Allocation Grant MCA05S028 and the Blue Waters petascale supercomputer system (UIUC).

## REFERENCES


(1) Hille, B. *Ion Channels of Excitable Membranes*, 3rd ed.; Sinauer: Sunderland, MA, 2001.

(2) Sui, H.; Han, B. G.; Lee, J. K.; Walian, P.; Jap, B. K. Structural basis of water-specific transport through the AQP1 water channel. *Nature* **2001**, *414*, 872−878.

(3) Bayley, H.; Cremer, P. S. Stochastic sensors inspired by biology. *Nature* **2001**, *413*, 226−230.

(4) Ghadiri, M. R.; Granja, J. R.; Buehler, L. K. Artificial transmembrane ion channels from self-assembling peptide nanotubes. *Nature* **1994**, *369*, 301−304.

(5) Montenegro, J.; Ghadiri, M. R.; Granja, J. R. Ion channel models based on self-assembling cyclic peptide nanotubes. *Acc. Chem. Res.* **2013**, *46*, 2955−2965.

(6) Sakai, N.; Matile, S. Synthetic Ion Channels. *Langmuir* **2013**, *29*, 9031−9040.

(7) Litvinchuk, S.; Tanaka, H.; Miyatake, T.; Pasini, D.; Tanaka, T.; Bollot, G.; Mareda, J.; Matile, S. Synthetic pores with reactive signal amplifiers as artificial tongues. *Nat. Mater.* **2007**, *6*, 576−580.

(8) Thomson, A. R.; Wood, C. W.; Burton, A. J.; Bartlett, G. J.; Sessions, R. B.; Brady, R. L.; Woolfson, D. N. Computational design of water-soluble α-helical barrels. *Science* **2014**, *346*, 485−488.

(9) Sakai, N.; Kamikawa, Y.; Nishii, M.; Matsuoka, T.; Kato, T.; Matile, S. Dendritic folate rosettes as ion channels in lipid bilayers. *J. Am. Chem. Soc.* **2006**, *128*, 2218−2219.

(10) Saha, T.; Dasari, S.; Tewari, D.; Prathap, A.; Sureshan, K. M.; Bera, A. K.; Mukherjee, A.; Talukdar, P. Hopping-mediated anion transport through a mannitol-based rosette ion channel. *J. Am. Chem. Soc.* **2014**, *136*, 14128−14135.

(11) Saha, T.; Gautam, A.; Mukherjee, A.; Lahiri, M.; Talukdar, P. Chloride transport through supramolecular barrel-rosette ion channels: Lipophilic control and apoptosis-inducing activity. *J. Am. Chem. Soc.* **2016**, *138*, 16443−16451.

(12) Langecker, M.; Arnaut, V.; Martin, T. G.; List, J.; Renner, S.; Mayer, M.; Dietz, H.; Simmel, F. C. Synthetic lipid membrane channels formed by designed DNA nanostructures. *Science* **2012**, *338*, 932−936.

(13) Burns, J. R.; Stulz, E.; Howorka, S. Self-assembled DNA nanopores that span lipid bilayers. *Nano Lett.* **2013**, *13*, 2351−2356.

(14) Burns, J. R.; Gopfrich, K.; Wood, J. W.; Thacker, V. V.; Keyser, U. F.; Howorka, S. Lipid-bilayer-spanning DNA nanopores with a bifunctional porphyrin anchor. *Angew. Chem., Int. Ed.* **2013**, *52*, 12069−12072.

(15) Burns, J. R.; Seifert, A.; Fertig, N.; Howorka, S. A biomimetic DNA-based channel for the ligand-controlled transport of charged molecular cargo across a biological membrane. *Nat. Nanotechnol.* **2016**, *11*, 152−156.

(16) Pinheiro, A. V.; Han, D.; Shih, W. M.; Yan, H. Challenges and opportunities for structural DNA nanotechnology. *Nat. Nanotechnol.* **2011**, *6*, 763−772.

(17) Yoo, J.; Aksimentiev, A. Molecular dynamics of membrane-spanning DNA channels: Conductance mechanism, electro-osmotic transport, and mechanical gating. *J. Phys. Chem. Lett.* **2015**, *6*, 4680−4687.

(18) Gopfrich, K.; Li, C. Y.; Mames, I.; Bhamidimarri, S. P.; Ricci, M.; Yoo, J.; Mames, A.; Ohmann, A.; Winterhalter, M.; Stulz, E.; Aksimentiev, A.; Keyser, U. F. Ion channels made from a single membrane-spanning DNA duplex. *Nano Lett.* **2016**, *16*, 4665−4669.

(19) Krishnan, S.; Ziegler, D.; Arnaut, V.; Martin, T. G.; Kapsner, K.; Henneberg, K.; Bausch, A. R.; Dietz, H.; Simmel, F. C. Molecular transport through large-diameter DNA nanopores. *Nat. Commun.* **2016**, *7*, 12787.

(20) (a) Fenniri, H.; Mathivanan, P.; Vidale, K. L.; Sherman, D. M.; Hallenga, K.; Wood, K. V.; Stowell, J. G. Helical Rosette Nanotubes: Design, Self-Assembly, and Characterization. *J. Am. Chem. Soc.* **2001**, *123*, 3854−3855. (b) Fenniri, H.; Deng, B. L.; Ribbe, A. E.; Hallenga, K.; Jacob, J.; Thiyagarajan, P. Entropically driven self-assembly of multichannel rosette nanotubes. *Proc. Natl. Acad. Sci. U. S. A.* **2002**, *99*, 6487−6492.

(21) (a) Beingessner, R.; Deng, B.-L.; Fanwick, P. E.; Fenniri, H. A Regioselective Approach to Trisubstituted 2 (or 6)-Arylaminopyrimidine-5-carbaldehydes and Their Application in the Synthesis of Structurally and Electronically Unique G∧C Base Precursors. *J. Org. Chem.* **2008**, *73*, 931−939. (b) Fenniri, H.; Tikhomirov, G. A.; Brouwer, D. H.; Bouatra, S.; El-Bakkari, M.; Yan, Z.; Cho, J.-Y.; Yamazaki, T. High Field Solid-State NMR Spectroscopy Investigation of $^{15}$N-Labeled Rosette Nanotubes: Hydrogen Bond Network and Channel-Bound Water. *J. Am. Chem. Soc.* **2016**, *138*, 6115−6118. (c) Hemraz, U. D.; El Bakkari, M.; Yamazaki, T.; Cho, J.-Y.; Beingessner, R. L.; Fenniri, H. Chiromers: Conformation-driven mirror-image supramolecular chirality isomerism identified in a new class of helical rosette nanotubes. *Nanoscale* **2014**, *6*, 9421−9427.

(22) Geng, J.; Kim, K.; Zhang, J.; Escalada, A.; Tunuguntla, R.; Comolli, L. R.; Allen, F. I.; Shnyrova, A. V.; Cho, K. R.; Munoz, D.; Wang, Y. M.; Grigoropoulos, C. P.; Ajo-Franklin, C. M.; Frolov, V. A.;

Noy, A. Stochastic transport through carbon nanotubes in lipid bilayers and live cell membranes. *Nature* **2014**, *514*, 612−615.
(23) Tunuguntla, R.; Henley, R. Y.; Yao, Y. C.; Pham, T. A.; Wanunu, M.; Noy, A. Enhanced water permeability and tunable ion selectivity in subnanometer carbon nanotube porins. *Science* **2017**, *357*, 792−796.
(24) $G = \sigma\left[\frac{4l}{\pi d^2} + \frac{1}{d}\right]$, where $G$ = conductance of the pore, $\sigma$ is bulk conductivity of electrolyte solution, $l$ is length of the pore, and $d$ is the diameter of the pore. For 1 M KCl, $\sigma$ is 110mS/cm, and for RNTP, $d$ is 1.1 nm. Therefore, the RNTP length can be derived as $l = 0.8635\left[\frac{12.1}{G} - 1\right]$, where $G$ is in nS and $l$ is in nm.
(25) Kasianowicz, J. J.; Bezrukov, S. M. Protonation dynamics of the $\alpha$-toxin ion channel from spectral analysis of pH-dependent current fluctuations. *Biophys. J.* **1995**, *69*, 94−105.
(26) Fragasso, A.; Pud, S.; Dekker, C. 1/f noise in solid-state nanopores is governed by access and surface regions. *Nanotechnology* **2019**, *30*, 395202.
(27) Parkin, W. M.; Drndic, M. Signal and noise in FET-nanopore Devices. *ACS Sens* **2018**, *3*, 313−319.
(28) Lopez, C. F.; Nielsen, S. O.; Moore, P. B.; Klein, M. L. Understanding nature's design for a nanosyringe. *Proc. Natl. Acad. Sci. U. S. A.* **2004**, *101*, 4431−4434.
(29) Gu, L. Q.; Braha, O.; Conlan, S.; Cheley, S.; Bayley, H. Stochastic sensing of organic analyte by a pore-forming protein containing a molecular adapter. *Nature* **1999**, *398*, 686−690.
(30) Kasianowicz, J. J.; Brandin, E.; Branton, D.; Deamer, D. W. Characterization of individual polynucleotide molecules using a membrane channel. *Proc. Natl. Acad. Sci. U. S. A.* **1996**, *93*, 13770−13773.
(31) Borzsonyi, G.; Beingessner, R. L.; Yamazaki, T.; Cho, J.; Myles, A. J.; Malac, M.; Egerton, R.; Kawasaki, M.; Ishizuka, K.; Kovalenko, A.; Fenniri, H. Water-soluble J-type rosette nanotubes with giant molar ellipticity. *J. Am. Chem. Soc.* **2010**, *132*, 15136−15139.
(32) Borzsonyi, G.; Alsbaiee, A.; Beingessner, R. L.; Fenniri, H. Synthesis of a tetracyclic G∧C scaffold for the assembly of rosette nanotubes with 1.7 nm inner diameter. *J. Org. Chem.* **2010**, *75*, 7233−7239.
(33) Piguet, F.; Ouldali, H.; Pastoriza-Gallego, M.; Manivet, P.; Pelta, J.; Oukhaled, A. Identification of single amino acid differences in uniformly charged homopolymeric peptides with aerolysin nanopore. *Nat. Commun.* **2018**, *9*, 966.
(34) Wilson, J.; Sarthak, K.; Si, W.; Gao, L.; Aksimentiev, A. Rapid and Accurate Determination of Nanopore Ionic Current Using a Steric Exclusion Model. *ACS Sens.* **2019**, *4*, 634−644.


https://dx.doi.org/10.1021/jacs.9b10993
*J. Am. Chem. Soc.* 2020, 142, 1680−1685